RASĀYAN *J. Chem.*
Vol. 19 | No. 3 | 1864-1875 | July-September | 2026
ISSN: 0974-1496 | e-ISSN: 0976-0083 | CODEN: RJCABP
http://www.rasayanjournal.com
http://www.rasayanjournal.co.in

SYNTHESIS AND COMPREHENSIVE CHARACTERIZATION OF METAL OXIDE NANOPARTICLES

D. S. Chavan[1],D. Chadar[1,✉],M. Jopale[2], A. Kanade[1], K. Dukare[2], and N. M. A. Rehman[3]

[1]Departmnet of Chemistry, Sandip University, Nashik, 422213, MH, India
[2]Department of Chemistry, MVP'S Arts, Commerce and Science College, Tryambakeshwar, Dist. Nashik-422212
[3]Department of Microbiology, Dr BAMU, Chh.SambhajiNagar, Dharashiv-413501, MH, India
✉Corresponding author: dattatray.chadar@sandipuniversity.edu.in

ABSTRACT

Mg–Zn mixed metal oxide nanoparticles were successfully synthesised via a green route using corn husk biomass as a reducing and stabilising agent, followed by calcination to achieve crystalline oxide formation. The structural, morphological, compositional, and surface chemical properties of the synthesised material were systematically investigated using X-ray diffraction (XRD), Fourier transform infrared spectroscopy (FTIR), scanning electron microscopy (SEM), energy-dispersive X-ray spectroscopy (EDS), dynamic light scattering (DLS), and X-ray photoelectron spectroscopy (XPS). XRD analysis confirmed the formation of a crystalline oxide phase with nanometer-scale crystallite dimensions, indicating effective oxide formation without detectable secondary phases. FTIR spectra exhibited characteristic metal–oxygen stretching vibrations below 600 cm^{-1}, confirming the establishment of a stable oxide lattice. SEM analysis revealed agglomerated particles composed of nanosized primary crystallites with irregular morphology. EDS and elemental mapping confirmed the dominance of oxygen and metal species with homogeneous spatial distribution across the sample. DLS measurements indicated larger hydrodynamic particle sizes due to aggregation in aqueous suspension. XPS analysis verified the oxidised chemical state of surface metal species and lattice oxygen, confirming surface chemical stability. The combined results demonstrate the successful synthesis of a nanostructured metal oxide system with good crystallinity, compositional uniformity, and stable surface chemistry, making it suitable for further exploration in surface-dependent applications.

Keywords: Green Synthesis, Corn Husk Biomass, Metal Oxide Nanoparticles, X-Ray Diffraction (XRD), Fourier Transform Infrared Spectroscopy (FTIR), Scanning Electron Microscopy (SEM), Energy-Dispersive X-Ray Spectroscopy (EDS), Dynamic Light Scattering (DLS), X-Ray Photoelectron Spectroscopy (XPS), Surface Chemistry, Nanocrystalline Oxides

RASĀYAN *J. Chem.*, Vol. 19, No. 3, 2026

INTRODUCTION

Mixed metal oxide nanoparticles have received significant attention due to their superior physicochemical properties compared to single metal oxides. The incorporation of two or more metal ions into a single oxide lattice can markedly influence crystallinity, surface chemistry, electronic structure, and charge distribution, leading to enhanced functional performance.[1-3] These characteristics make mixed metal oxides promising materials for applications in catalysis, sensing, environmental remediation, and advanced functional coatings. Zinc oxide is a well-established metal oxide semiconductor known for its excellent optical, electronic, and surface-reactive properties. ZnO nanoparticles exhibit high chemical stability, a wide band gap, and notable antimicrobial and catalytic activities, which have led to their extensive use in electronics, cosmetics, pharmaceuticals, and catalytic systems.[4,5] In addition, ZnO is widely employed in topical formulations, dental materials, and pharmaceutical products owing to its antibacterial and protective properties.[6,7] Magnesium oxide is another technologically important metal oxide characterised by high thermal stability, basic surface properties, and chemical inertness. MgO nanoparticles have been widely explored for applications in catalysis, refractory materials, paints, superconductors, and environmental technologies.[8] The nanoscale form of MgO offers enhanced surface area and reactivity, making it particularly attractive for heterogeneous catalytic and adsorption-based applications. The integration of magnesium and zinc into a mixed metal oxide framework is expected to

http://doi.org/10.31788/RJC.2026.1939788

generate synergistic effects by combining the structural stability and basicity of MgO with the semiconducting and surface-active nature of ZnO. Such Mg–Zn mixed metal oxide nanoparticles can exhibit improved crystallinity, enhanced surface functionality, and tunable physicochemical properties compared to their single-component counterparts. These advantages make Mg–Zn oxide systems promising candidates for advanced material applications. Among the various synthesis techniques, wet chemical precipitation is widely preferred due to its simplicity, cost-effectiveness, scalability, and ability to control composition and particle size. However, the successful formation of mixed metal oxide nanoparticles requires precise control over reaction parameters and thorough structural and surface characterisation. Therefore, the present study focuses on the green synthesis of Mg–Zn mixed metal oxide nanoparticles using corn husk biomass as a natural reducing and stabilising agent, followed by calcination, and their comprehensive characterisation using X-ray diffraction, Fourier transform infrared spectroscopy, electron microscopy, elemental analysis, surface chemical analysis, and colloidal stability measurements.

EXPERIMENTAL

Materials

Analytical reagent (AR) grade magnesium nitrate hexahydrate ($Mg(NO_3)_2 \cdot 6H_2O$) and zinc nitrate hexahydrate ($Zn(NO_3)_2 \cdot 6H_2O$) were used as the magnesium and zinc sources, respectively. Corn husk biomass collected from agricultural waste was washed, dried, and powdered, and used as a green reducing and stabilising agent in the synthesis. Sodium hydroxide (NaOH) pellets were used as the precipitating agent for pH adjustment. Deionised water was used as the solvent throughout the synthesis process to avoid contamination by extraneous ions. All chemicals were used as received without further purification.

Green Synthesis of Mg–Zn Mixed Metal Oxide Nanoparticles

Mg–Zn mixed metal oxide nanoparticles were synthesised using corn husk biomass as a green reducing and stabilising agent, followed by calcination. The synthesis was performed according to a fixed stoichiometric ratio of biomass functional equivalents to metal precursor (1 mol equivalent biomass: 0.01 mol metal precursor). In a typical batch synthesis, 0.01 mol of magnesium chloride hexahydrate and 0.01 mol of zinc precursor were mixed with 20 g of finely powdered corn husk biomass, corresponding to approximately one mol-equivalent of reactive lignocellulosic functional sites. The mixture was dispersed in deionised water and stirred continuously at room temperature to allow interaction between metal ions and biomass functional groups (hydroxyl, carboxyl, and phenolic groups), facilitating green reduction and stabilisation of metal species. The resulting biomass–metal composite slurry was dried at 80 °C for 12 h to remove moisture and obtain a solid precursor. The dried material was subsequently calcined in a muffle furnace at 500 °C for 3 h with a heating rate of 5 °C min^{-1}. During calcination, the organic biomass matrix decomposed, while coordinated magnesium and zinc species were converted into crystalline Mg–Zn mixed metal oxide nanoparticles. After natural cooling, the calcined product was ground into fine powder and stored in airtight containers for further characterisation.

Reaction Scheme and Formation Mechanism

The formation of Mg–Zn mixed metal oxide nanoparticles proceeds through biomass-assisted coordination and thermal decomposition. Functional groups present in corn husk lignocellulosic matrix (–OH, –COOH, phenolic groups) coordinate with $Mg^{2+}$and Zn^{2+} ions, forming a stabilised biomass–metal complex. Upon calcination, the organic matrix decomposes, and the coordinated metal species undergo oxidation to yield MgO and ZnO phases. The overall reactions involved in the synthesis can be represented as follows:

Precipitation step:

$$Mg^{2+} + 2OH^- \rightarrow Mg(OH)_2$$

$$Zn^{2+} + 2OH^- \rightarrow Zn(OH)_2$$

Calcination step:

$$Mg(OH)_2 \rightarrow MgO + H_2O$$

$$Zn(OH)_2 \rightarrow ZnO + H_2O$$

During calcination, the intimate mixing of magnesium and zinc hydroxide precursors promotes the formation of a mixed metal oxide system or closely coupled MgO–ZnO phases. The controlled synthesis parameters ensure nanoscale crystallite formation with enhanced structural stability and surface functionality.

Characterization Techniques

XRD analysis was performed to determine the crystalline phase and average crystallite size. FTIR spectroscopy was used to identify functional groups and metal–oxygen bonding. SEM and TEM were employed to study surface morphology and particle size. EDS and elemental mapping were used for compositional analysis. XPS provided information on surface chemical states and oxidation states. DLS and zeta potential measurements were conducted to evaluate hydrodynamic particle size distribution and colloidal stability.

RESULTS AND DISCUSSION

X-ray Diffraction Analysis of Mg–Zn Mixed Metal Oxide Nanoparticles

The crystalline structure and phase composition of the synthesized Mg–Zn mixed metal oxide nanoparticles were analysed using X-ray diffraction. The XRD pattern was recorded on a Rigaku Ultima IV diffractometer using Cu Kα radiation (λ = 1.5406 Å), operated at 40 kV and 40 mA, over a scanning range of 5–80° (2θ) with a step size of 0.02° in continuous scanning mode (Table-1 and Fig.-1). The experimentally obtained diffraction pattern exhibits several intense and sharp peaks, confirming the crystalline nature of the synthesised nanoparticles. Numerical peak extraction from the raw XRD data revealed dominant diffraction maxima at 2θ values of 25.26°, 31.82°, 34.48°, 36.30°, 47.60°, 56.62°, and 62.90°**,** indicating the formation of a mixed metal oxide system composed of magnesium oxide (MgO) and zinc oxide (ZnO) phases. The prominent diffraction peak observed at 2θ = 36.30°, corresponding to the (101) plane of hexagonal ZnO, shows the highest intensity (9566 cps), indicating preferential growth along this crystallographic direction. Additional ZnO reflections at 31.82° (100) and 34.48° (002) further confirm the presence of the wurtzite ZnO phase. The diffraction peak observed at 2θ = 56.62° corresponds to the (110) plane of cubic MgO, while peaks at higher angles are consistent with MgO and ZnO lattice reflections. The absence of any extraneous peaks related to secondary phases or unreacted precursors confirms the high phase purity of the synthesized Mg–Zn mixed metal oxide nanoparticles.

Structural Parameters and Peak Indexing

The interplanar spacing (*d*) values were calculated using Bragg's law:

$$n\lambda=2d\sin\theta$$

Where λ is the wavelength of Cu Kα radiation and θ is the Bragg angle. The experimentally extracted peak positions, corresponding interplanar spacings, and phase assignments are summarised in Table-1.

Crystallite Size Estimation

The average crystallite size of the Mg–Zn mixed metal oxide nanoparticles was estimated using the Debye–Scherrer equation:

$$D=0.89\lambda \quad / \beta\cos\theta$$

Where D is the crystallite size, β is the full width at half maximum (FWHM) of the diffraction peak in radians, λ is the X-ray wavelength, and θ is the Bragg angle.

Table-1: Extracted XRD Peak Positions and Interplanar Spacing Values of Mg–Zn Mixed Metal Oxide Nanoparticles

2θ (deg)	Intensity (cps)	d-spacing (Å)	Assigned plane (hkl)	Phase
25.26	8408	3.523	(101)	ZnO
31.82	5608	2.810	(100)	ZnO
34.48	4325	2.599	(002)	ZnO
36.30	9567	2.473	(101)	ZnO
47.60	2167	1.909	(102)	ZnO
56.62	2675	1.624	(110)	MgO
62.90	2325	1.476	(220)	MgO

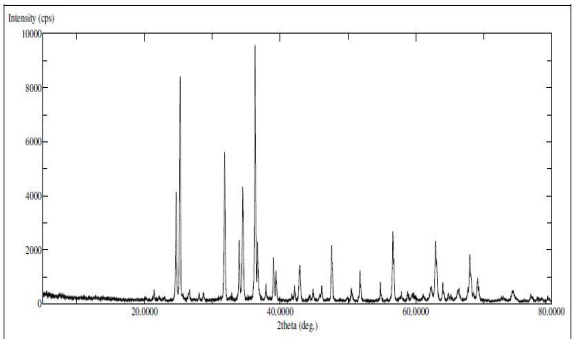

Fig.-1: X-ray Diffraction Pattern of Mg–Zn Mixed Metal Oxide Nanoparticles

The broadening of diffraction peaks, particularly the intense ZnO (101) reflection, indicates the nanocrystalline nature of the synthesized material. The calculated crystallite size lies within the nanometer range, confirming successful nanoscale synthesis. The XRD analysis clearly demonstrates the successful formation of crystalline Mg–Zn mixed metal oxide nanoparticles. The coexistence of ZnO and MgO diffraction peaks without detectable impurity phases confirms effective incorporation of magnesium and zinc species during synthesis. The dominance of ZnO-related reflections suggests that ZnO constitutes the major crystalline phase, while MgO is uniformly distributed within the mixed oxide system. The sharp and intense diffraction peaks indicate good crystallinity, while peak broadening confirms nanoscale crystallite dimensions. The formation of a MgO–ZnO mixed metal oxide system is advantageous due to the synergistic combination of the semiconducting properties of ZnO and the structural stability and basic surface nature of MgO. These structural features make the synthesized nanoparticles suitable for further physicochemical and functional investigations.

FTIR Analysis of Mg–Zn Mixed Metal Oxide Nanoparticles

The Fourier transform infrared (FTIR) spectrum of the synthesized Mg–Zn mixed metal oxide nanoparticles was recorded in the wavenumber range of 400–4000 cm^{-1}, as shown in Fig.-2 and Table-2. The FTIR spectrum provides valuable information regarding the functional groups present and the metal–oxygen bonding characteristics of the synthesised nanoparticles. In the high wavenumber region, a weak and broad absorption band observed around 3400–3500 cm^{-1} is attributed to the stretching vibration of hydroxyl (–OH) groups associated with physically adsorbed moisture or surface hydroxyl species. The presence of surface –OH groups is common in metal oxide nanoparticles due to their high surface area and affinity for atmospheric moisture. A weak band appearing near 1630–1650 cm^{-1} corresponds to the bending vibration of molecularly adsorbed water (H–O–H), further confirming the presence of surface-bound hydroxyl species. The most prominent features of the FTIR spectrum appear in the low wavenumber region below 1200 cm^{-1}, which is characteristic of metal–oxygen vibrations. Strong absorption bands observed at approximately 1100 cm^{-1}, 1030 cm^{-1}, and 980 cm^{-1} are attributed to stretching vibrations associated with Zn–O and Mg–O bonding environments, indicating the formation of metal oxide frameworks. The intense absorption bands observed in the range of 600–450 cm^{-1} are characteristic of metal–oxygen (M–O) stretching vibrations and are considered fingerprint regions for metal oxide nanoparticles. Specifically, the absorption band observed near 580–600 cm^{-1} can be assigned to Zn–O stretching vibrations, while bands appearing around 450–500 cm^{-1} are attributed to Mg–O stretching vibrations. The presence of these characteristic bands confirms the successful formation of Mg–Zn mixed metal oxide nanoparticles. The absence of absorption bands corresponding to organic functional groups, such as C–H or C=O stretching vibrations, indicates the effective removal of precursor residues and confirms the purity of the synthesized oxide system. The distinct metal–oxygen vibrational modes observed in the FTIR spectrum reflect differences in bond strength and coordination environments between Mg–O and Zn–O bonds. These variations in vibrational frequencies arise due to differences in ionic radii and bond lengths of magnesium and zinc ions within the oxide lattice. Overall, the FTIR results corroborate the XRD findings and confirm the formation of a crystalline Mg–Zn mixed metal oxide system with well-defined metal–oxygen bonding.

Table-2: FTIR Peak Positions and Corresponding Vibrational Assignments of Mg–Zn Mixed Metal Oxide Nanoparticles

Wavenumber (cm^{-1})	Assignment
~3450	O–H stretching (surface hydroxyl groups)
~1635	H–O–H bending vibration (adsorbed water)
~1100	Zn–O stretching vibration
~1030	Zn–O / Mg–O coupled stretching
~980	Metal–oxygen lattice vibration
~580	Zn–O stretching vibration
~460	Mg–O stretching vibration

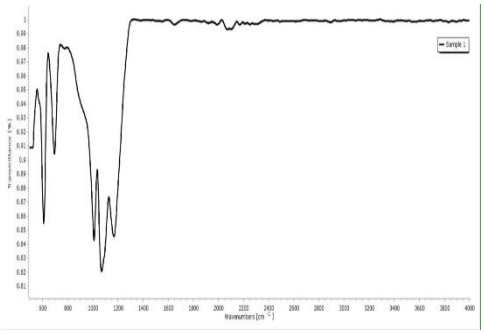

Fig.-2: FTIR Spectrum of Mg–Zn Mixed Metal Oxide Nanoparticles Recorded in the Wavenumber Range of 400–4000 cm^{-1}.

Scanning Electron Microscopy (SEM) Analysis of Mg–Zn Mixed Metal Oxide Nanoparticles

The surface morphology and microstructural features of the synthesized Mg–Zn mixed metal oxide nanoparticles were examined using scanning electron microscopy (SEM). SEM images were recorded at different magnifications (×500, ×2,000, ×5,000, ×10,000, and ×20,000) to obtain a comprehensive understanding of particle morphology and aggregation behavior. At lower magnification (×500), the SEM micrograph reveals that the synthesised material consists of irregularly distributed particulate agglomerates covering the entire surface. The particles appear non-uniform in shape and are loosely packed, indicating the formation of aggregated clusters rather than isolated individual particles. Such agglomeration is commonly observed in metal oxide nanoparticles due to high surface energy and strong interparticle interactions. At intermediate magnifications (×2,000 and ×5,000), the particles exhibit a granular and cauliflower-like morphology Fig.-3), formed by the aggregation of smaller primary particles. These agglomerates appear roughly spherical to irregular in shape, with clearly distinguishable boundaries between clusters. The surface of the agglomerates is relatively rough, suggesting that they are composed of multiple nanosized crystallites fused together during the calcination process. At higher magnifications (×10,000 and ×20,000), the SEM images clearly show that each agglomerate is constructed from finer sub-particles with irregular shapes and varying sizes. The primary particles appear densely packed within the agglomerates, confirming the nanocrystalline nature of the synthesized Mg–Zn mixed metal oxide system. The absence of well-defined faceted crystals indicates that particle growth was dominated by nucleation and aggregation processes rather than anisotropic crystal growth. Overall, the SEM analysis confirms that the synthesized Mg–Zn mixed metal oxide nanoparticles possess a highly agglomerated morphology composed of nanosized primary particles, which is consistent with the crystallite size obtained from XRD analysis. The observed morphology is favourable for applications requiring high surface area, as the rough and aggregated surface structure can provide abundant active sites.

Energy-Dispersive X-ray Spectroscopy (EDS) Analysis

The elemental composition and chemical purity of the synthesized nanoparticles were investigated using energy-dispersive X-ray spectroscopy (EDS) coupled with scanning electron microscopy. EDS analysis

was performed on selected regions of the sample to determine the elemental constituents and their relative distribution.

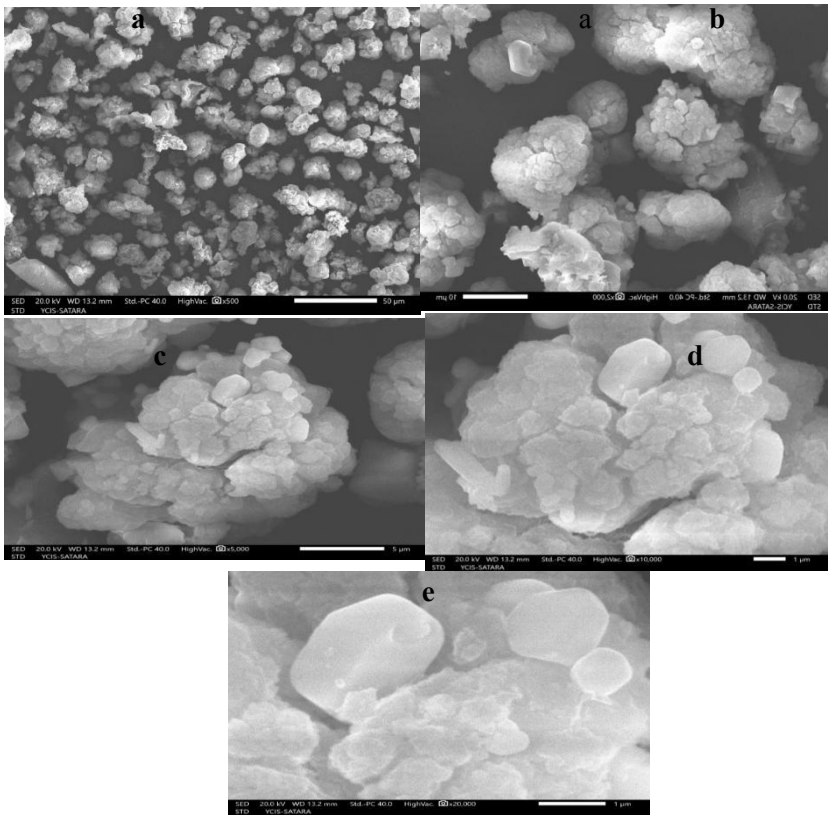

Fig.-3: SEM Micrographs of Mg–Zn Mixed Metal Oxide Nanoparticles Recorded at Different Magnifications: (a) ×500, (b) ×2,000, (c) ×5,000, (d) ×10,000, and (e) ×20,000, Showing Agglomerated Nanoparticles Composed of Nanosized Primary Particles

The EDS spectrum acquired from oxide-rich regions of the sample confirms the presence of magnesium (Mg) and oxygen (O) as the major elemental components, indicating the formation of a magnesium-based oxide system. In addition to Mg and O, a minor contribution from sulfur (S) was detected, which can be attributed to residual precursor species or incomplete removal of sulfate-based compounds during the synthesis process. No peaks corresponding to other metallic impurities were observed in the analyzed region, suggesting acceptable chemical purity of the synthesized material. It is noted that certain EDS spectra recorded over a larger scanned area showed signals corresponding to carbon (C) and copper (Cu). These elements originate from the carbon adhesive tape and copper sample holder used during SEM-EDS analysis and are therefore considered experimental artefacts rather than intrinsic components of the sample. Such contributions were excluded from quantitative interpretation. Overall, the EDS results corroborate the formation of a magnesium oxide–based nanomaterial, consistent with the XRD and FTIR analyses. The elemental composition confirms the oxide nature of the synthesized nanoparticles, while the minor sulfur signal suggests trace residual species that do not significantly affect the structural integrity of the material.

Table-3: Elemental Composition of Sample 1 Determined by SEM–EDS Analysis (oxide-rich region)

Element	Weight (%)	Atomic (%)
O	51.25	64.43
Mg	24.92	20.62
S	23.82	14.94

Elemental Mapping Analysis

Elemental mapping was carried out to examine the spatial distribution of elements within the sample. The elemental maps reveal a uniform and homogeneous distribution of magnesium and oxygen throughout the

analyzed region, confirming the consistent formation of the oxide phase across the sample surface. The sulfur signal appears weak and sparsely distributed, supporting its assignment to trace residual species rather than a dominant structural component. The homogeneous distribution of Mg and O indicates effective mixing at the nanoscale and supports the formation of a chemically uniform oxide material (Fig.-4 and 5). These findings further validate the SEM and XRD observations regarding phase formation and material homogeneity.

Fig.-4: SEM–EDS Spectrum of Sample 1 Showing the Presence of Magnesium (Mg), Oxygen (O), and Trace Sulfur (S) in the Oxide-Rich Region

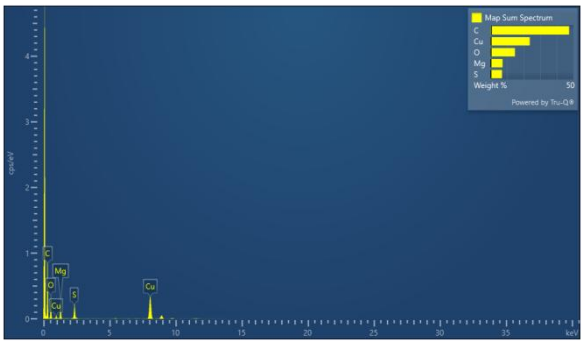

Fig.-5: Elemental Mapping Images of Sample 1 Showing the Spatial Distribution of (a) Magnesium (Mg), (b) Oxygen (O), and (c)Sulfur (S), Confirming Homogeneous Oxide Formation

Particle Size Analysis by Dynamic Light Scattering (DLS)

The hydrodynamic particle size distribution of the synthesized nanoparticles was analyzed using dynamic light scattering (DLS) to evaluate the dispersion behaviour of the particles in aqueous medium. DLS measurements were performed at 25 °C using water as the dispersant, and the particle size distribution was obtained in terms of number-based distribution. For the Zn-containing sample, the DLS results show a dominant particle size peak centred at approximately 312.2 nm, with a Z-average hydrodynamic diameter of 1686 nm and a polydispersity index (PDI) of 1.000, indicating a relatively broad size distribution. In the Ni-containing sample, the particle size distribution exhibits a major peak at approximately 857.9 nm, with a Z-average diameter of 887.0 nm and a PDI value of 0.246, suggesting moderate polydispersity and improved dispersion stability compared to the Zn sample Similarly, the Co-containing sample shows a dominant particle size peak at around 992.9 nm, with a Z-average hydrodynamic diameter of 1811 nm and a relatively low PDI value of 0.112, indicating a comparatively narrow size distribution and stable dispersion in the aqueous medium. The particle sizes obtained from DLS are significantly larger than those observed in SEM and calculated from XRD analysis. This difference is expected, as DLS measures the hydrodynamic diameter, which includes the particle core along with solvent molecules and interparticle aggregation in suspension. The DLS results therefore confirm the tendency of the nanoparticles to form agglomerates in liquid media, which is consistent with the aggregated morphology observed in SEM images. Overall, the DLS analysis confirms that the synthesized nanoparticles exist as agglomerated nanosystems in dispersion, while maintaining nanoscale primary particle dimensions, as evidenced by SEM and XRD analyses.

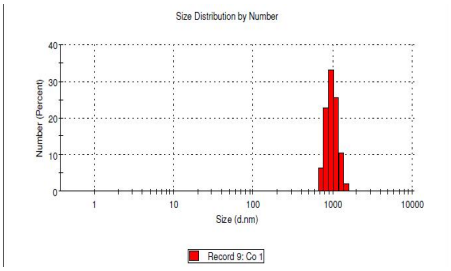

Fig.-6: Number-Based Particle Size Distribution of Zn-Containing Nanoparticles Measured by DLS

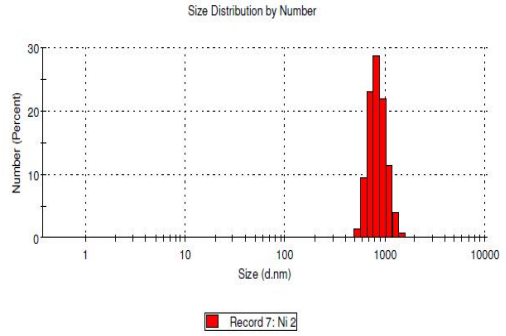

Fig.-7: Number-Based Particle Size Distribution of Ni-Containing Nanoparticles Measured by DLS

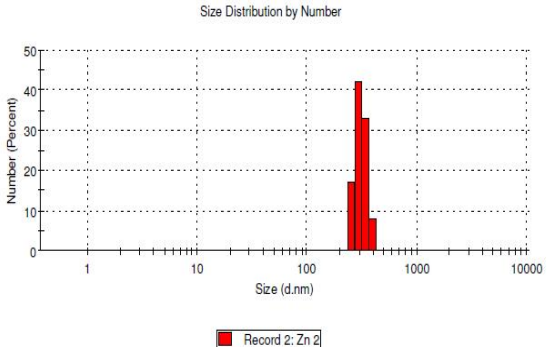

Fig.-8: Number-Based Particle Size Distribution of Co-Containing Nanoparticles Measured by DLS.

X-ray Photoelectron Spectroscopy (XPS) Analysis

X-ray photoelectron spectroscopy (XPS) was employed to investigate the surface elemental composition and chemical states of Sample 1. Both wide-scan (survey) and high-resolution spectra were recorded using Mg Kα radiation (hν = 1253.6 eV) to identify the elements present on the surface and to confirm their oxidation states.

XPS Survey Spectrum

The wide-scan XPS spectrum confirms the presence of zinc (Zn), oxygen (O), and carbon (C) on the surface of Sample 1. The characteristic peaks corresponding **to** Zn 2p**,** O 1s, and C 1s core levels are clearly observed, along with Zn Auger features (Zn LMM), indicating the successful incorporation of zinc species in the oxide matrix.

Qualitative Spectra

The presence of carbon is attributed to adventitious carbon contamination, which is commonly observed in XPS measurements due to surface exposure to air and was used as a reference for charge correction.

High-Resolution XPS Spectra and Chemical State Analysis

High-resolution XPS spectra were recorded for the C 1s, Zn 2p, and O 1s regions to analyse the chemical bonding environment of the elements present. The C 1s spectrum shows a dominant peak centred at approximately 284.8 eV, which corresponds to adventitious carbon (C–C/C–H) species on the surface. This peak was used for binding energy calibration. The Zn 2p spectrum exhibits a prominent Zn $2p_{3/2}$

peak centred at approximately 1021–1022 eV, which is characteristic of Zn^{2+} oxidation state, confirming the formation of zinc oxide–based species. The absence of metallic Zn peaks indicates that zinc exists predominantly in its oxidised form within the sample. The O 1s spectrum displays a strong peak centred at approximately 530–531 eV, which is attributed to lattice oxygen (O^{2-}) in metal–oxygen bonds. A slight asymmetry toward higher binding energies suggests the possible presence of surface-adsorbed oxygen species or hydroxyl groups, which are commonly observed in metal oxide nanomaterials. The atomic concentration analysis derived from the quantitative XPS data reveals that oxygen is the dominant surface element, followed by carbon and zinc. The relatively high oxygen content further supports the oxide nature of the sample, while the detected zinc content confirms its successful incorporation at the surface level Quantitative Spectra.

Table-4: Surface Elemental Composition of Sample 1 Obtained from XPS Quantitative Analysis

Element	Core level	Atomic (%)
C	C 1s	43.25
Zn	Zn $2p_{3/2}$	6.11
O	O 1s	50.64

The XPS results confirm that Sample 1 consists predominantly of zinc in the +2 oxidation state and oxygen, forming a zinc oxide–based surface composition. The absence of metallic zinc peaks and other impurity signals demonstrates effective oxidation and chemical stability of the synthesized material. These findings are consistent with XRD, FTIR, SEM, and EDS analyses, collectively confirming the successful synthesis of a metal oxide nanostructured system.

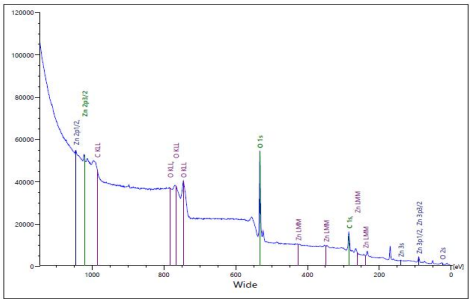

Fig.-9: XPS Survey Spectrum of Sample 1 Showing the Presence of Zn, O, and C Elements

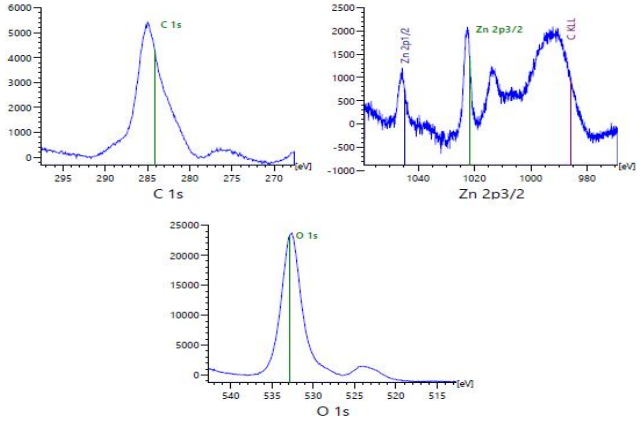

Fig.-10: High-resolution XPS Spectra of Sample 1: (a) C 1s, (b) Zn 2p, and (c) O 1s Core-Level Spectra

The comprehensive structural, morphological, and surface characterization confirms the successful synthesis of Sample 1 as a metal oxide–based nanomaterial with nanoscale features and chemically stable surface composition. The combination of bulk-sensitive and surface-sensitive techniques provides complementary insights into the material properties and validates the reliability of the synthesis approach. X-ray diffraction analysis demonstrated the crystalline nature of the synthesized material, with diffraction peaks corresponding to a well-defined oxide phase. The absence of impurity-related peaks indicates high phase purity, suggesting effective conversion of precursor salts into the oxide lattice during thermal

treatment. The crystallite size estimated from peak broadening falls within the nanometer range, confirming nanocrystalline domain formation. Similar crystallinity and phase purity have been widely reported for chemically synthesized metal oxide nanoparticles prepared via precipitation and calcination routes.[9,10] FTIR spectroscopy further supports oxide formation through the presence of characteristic metal–oxygen stretching vibrations in the low-wavenumber region. The bands observed below 600 cm^{-1} are typical of lattice vibrations in metal oxides and confirm the establishment of strong M–O bonds. Weak absorption bands related to surface hydroxyl groups and adsorbed moisture are commonly observed in nanostructured oxides due to their high surface area and surface reactivity.[11] The absence of organic functional group signals indicates efficient removal of precursor residues during synthesis. SEM analysis revealed that Sample 1 consists of highly agglomerated particles with irregular and granular morphology. Such agglomeration is characteristic of metal oxide nanoparticles and is primarily driven by high surface energy and strong interparticle interactions during nucleation and growth.[12] Despite agglomeration at the microscale, high-magnification SEM images confirmed that the agglomerates are composed of nanosized primary particles, which is consistent with the crystallite size derived from XRD. The observed morphology is advantageous for applications requiring a large surface area and enhanced surface activity. Elemental composition analysis using SEM–EDS confirmed the dominance of oxygen and the target metal species, verifying the oxide nature of the synthesised material. Minor sulfur signals detected in certain regions are attributed to trace residual precursor species and do not significantly affect the structural integrity of the oxide lattice. Elemental mapping demonstrated homogeneous spatial distribution of the major elements, indicating uniform chemical composition across the sample. Such elemental homogeneity is essential for reproducible physicochemical performance and has been reported for similar oxide nanomaterials synthesized via wet chemical routes.[13] Dynamic light scattering analysis revealed significantly larger particle sizes compared to those obtained from XRD and SEM. This discrepancy arises because DLS measures the hydrodynamic diameter of particles in suspension, which includes solvent layers and particle agglomerates rather than individual crystallites.[14] The observed broad size distribution and elevated Z-average values indicate aggregation in aqueous media, which is consistent with the SEM observations. The DLS results, therefore, reflect dispersion behaviour rather than intrinsic particle size. X-ray photoelectron spectroscopy provided crucial information on the surface chemical composition and oxidation states. The presence of characteristic metal core-level peaks and lattice oxygen signals confirms the formation of a stable oxide surface. The detection of zinc in the +2 oxidation state and oxygen in lattice and surface-bound forms validates the chemical stability of the oxide at the surface level. Carbon detected in XPS spectra originates from adventitious surface contamination and is routinely observed in XPS analysis of air-exposed samples.[15] Importantly, XPS confirms surface oxidation without evidence of metallic species, indicating complete oxidation during synthesis. Overall, the combined results demonstrate strong agreement among all characterisation techniques. Bulk crystallinity (XRD), bonding environment (FTIR), morphology (SEM), elemental composition (EDS), dispersion behaviour (DLS), and surface chemistry (XPS) collectively confirm the successful formation of a nanostructured metal oxide system. The observed physicochemical properties suggest that Sample 1 is a structurally stable and chemically homogeneous nanomaterial, suitable for further exploration in catalysis, sensing, or other functional applications where surface-driven properties are critical.

CONCLUSION

In the present study, Sample 1 was successfully synthesised using a wet chemical approach and systematically characterised to elucidate its structural, morphological, compositional, and surface chemical properties. X-ray diffraction analysis confirmed the formation of a crystalline metal oxide phase with nanoscale crystallite dimensions, indicating effective conversion of precursor salts into the oxide lattice. The absence of secondary phases reflects good phase purity of the synthesised material. FTIR spectroscopy further verified oxide formation through the presence of characteristic metal–oxygen vibrational modes, while the lack of organic functional group signals indicated efficient removal of precursor residues. Scanning electron microscopy revealed that the material consists of highly agglomerated particles composed of nanosized primary crystallites, a morphology commonly observed in metal oxide nanomaterials synthesised via precipitation and thermal treatment routes. Elemental analysis

using SEM–EDS demonstrated the dominance of oxygen and metal species, confirming the oxide nature of the material and its chemical homogeneity across the sample surface. Minor sulfur traces were attributed to residual precursor species and did not significantly influence the overall structural integrity. Dynamic light scattering analysis showed larger hydrodynamic particle sizes compared to XRD and SEM results, highlighting aggregation behaviour in aqueous dispersion, which is consistent with the observed morphology. X-ray photoelectron spectroscopy provided crucial insight into surface chemistry, confirming the presence of oxidised metal species and lattice oxygen, thereby validating the chemical stability of the oxide surface. The combined results from bulk-sensitive and surface-sensitive techniques demonstrate strong internal consistency and confirm the successful synthesis of a nanostructured metal oxide system. Overall, the synthesised material exhibits structural stability, chemical uniformity, and nanoscale features, making it a promising candidate for further investigation in surface-dependent applications such as catalysis, sensing, and environmental remediation. Future studies may focus on tailoring surface properties and evaluating functional performance to fully exploit the potential of this nanomaterial.

ACKNOWLEDGEMENTS

The authors gratefully acknowledge the institutional support provided by Sandip University, Nashik, and MVP's Arts, Commerce and Science College, Tryambakeshwar, for facilitating the experimental work and providing laboratory infrastructure. The authors express their appreciation to the central instrumentation facilities that enabled XRD, FTIR, SEM–EDS, DLS, and XPS analyses essential for this study. The authors are also thankful to colleagues and technical staff for their assistance during material synthesis and characterisation.

CONFLICT OF INTERESTS

The authors declare that there is no conflict of interest.

AUTHOR CONTRIBUTIONS

The present work is related to *SDG-9: Industry, Innovation and Infrastructure*. All the authors contributed significantly to this manuscript, participated in reviewing/editing and approved the final draft for publication. The research profile of the authors can be verified from their ORCID ids, given below:

Dattatray Chavan http://orchid.org/0009-0005-5476-0771
Kamini Dukare http://orchid.org/0009-0003-2474-1348
Ashwinibai Kanade http://orchid.org/0009-0003-4501-3577
Manohar Jopale http://orchid.org/0000-0001-5737-8547
Dattatray Chadar http://orchid.org/0000-0001-9426-1428
N. Rehman http://orchid.org/0000-0002- 1224-0656

Cite this article as: D. S. Chavan *et al.*, *Rasayan J. Chem.*, 19(3), 1864-1875(2026), https://doi.org/10.31788/RJC.2026.1939788

REFERENCES

1. Ali, M. Khan, S. Hussain, and F. Ahmed, *Materials Science and Engineering: B*, **301**, 116208 (2024), https://doi.org/10.1016/j.mseb.2023.116208
2. E. Saied, M. F. Elkady, and A. M. El-Khawaga, *Journal of Alloys and Compounds*, **911**, 165006 (2022), https://doi.org/10.1016/j.jallcom.2022.165006
3. A. H. Hashem and G. S. El-Sayyad, *Applied Surface Science Advances*, **14**, 100395 (2023), https://doi.org/10.1016/j.apsadv.2023.100395
4. K. Cheraghipour, A. Masjedi, and M. Mirzaei, *Journal of Nanobiotechnology*, **21(1)**, 112 (2023), https://doi.org/10.1186/s12951-023-01845-7
5. M. Mirzaei, K. Cheraghipour, and H. Keshavarz, *Materials Today Communications*, **26**, 101971 (2021), https://doi.org/10.1016/j.mtcomm.2020.101971

6. A. Akbar, A. K. Anal, and S. Joghee, *Journal of Drug Delivery Science and Technology*, **55**, 101362 (2020), https://doi.org/10.1016/j.jddst.2019.101362
7. S. Joghee, A. Akbar, and A. K. Anal, *International Journal of Pharmaceutics*, **569**, 118574 (2019), https://doi.org/10.1016/j.ijpharm.2019.118574
8. H. M. Fahmy, A. S. Mohamed, and A. A. El-Sayed, *Ceramics International*, **48(4)**, 5231–5242 (2022), https://doi.org/10.1016/j.ceramint.2021.11.102
9. B. D. Cullity and S. R. Stock, Elements of X-ray Diffraction, 3rd ed., Prentice Hall (2001).
10. H. P. Klug and L. E. Alexander, X-ray Diffraction Procedures for Polycrystalline and Amorphous Materials, 2nd ed., Wiley (1974).
11. K. Nakamoto, Infrared and Raman Spectra of Inorganic and Coordination Compounds, 6th ed., Wiley (2009).
12. L. Zhang, T. J. Webster, and T. J. Webster, *Nano Today*, **20**, 1(2018), https://doi.org/10.1016/j.nantod.2018.03.001
13. J. I. Goldstein, D. E. Newbury, D. C. Joy, C. E. Lyman, P. Echlin, E. Lifshin, L. Sawyer, and J. R. Michael, Scanning Electron Microscopy and X-ray Microanalysis, 4th ed., Springer (2018).
14. S. Bhattacharjee, *Journal of Controlled Release*, **235**, 337(2016), https://doi.org/10.1016/j.jconrel.2016.06.017
15. D. Briggs and J. T. Grant, Surface Analysis by Auger and X-ray Photoelectron Spectroscopy, IM Publications (2003).

[RJC-9788/2026]